Journal of
Water & Climate Change

Check for updates

IWA PUBLISHING

© 2022 The Authors

Journal of Water and Climate Change Vol 13 No 2, 684 doi: 10.2166/wcc.2021.241

Disaggregation of future GCMs to generate IDF curves for the assessment of urban floods

H. Tayşi [a,*] and M. Özger [b]

[a] Faculty of Engineering, Department of Civil Engineering, Gebze Technical University, Gebze, Kocaeli 41400, Turkey
[b] Faculty of Civil Engineering, Department of Hydraulics and Water Resources Engineering, Istanbul Technical University, Sariyer, Istanbul 34467, Turkey
*Corresponding author. E-mail: h.taysi@gtu.edu.tr

HT, 0000-0002-4302-7364; MÖ, 0000-0001-9812-9918

ABSTRACT

Urbanization and industrialization cause an increase in greenhouse gas emissions, which in turn causes changes in the atmosphere. Climate change is causing extreme rainfalls and these rainfalls are getting stronger day after day. Floods are threatening urban areas, and short-duration rainfall and outdated drainages are responsible for urban floods. Intensity–Duration–Frequency (IDF) curves are crucial for both drainage system design and assessment of flood risk. Once IDF curves are determined from historical data, they are assumed to be stationary. However, IDF curves must be non-stationary and time varying based on preparation for extreme events. This study generates future IDF curves with short-duration rainfalls under climate change. To represent future rainfall, an ensemble of four Global Climate Models generated under Representative Concentration Pathways (RCP) 4.5 and 8.5 were used in this study. A new approach to the HYETOS disaggregation model was applied to disaggregate daily future rainfall into sub-hourly using disaggregation parameters of hourly measured rainfalls. Hence, sub-hourly future rainfalls will be obtained capturing historical rainfall patterns instead of random rainfall characteristics. Finally, historical and future IDF curves were compared. The study concludes that increases in short-duration rainfalls will be highly intensified in both the near and distant futures with a high probability.

Key words: climate change, disaggregation, GCM, IDF curves, RCP, urban floods

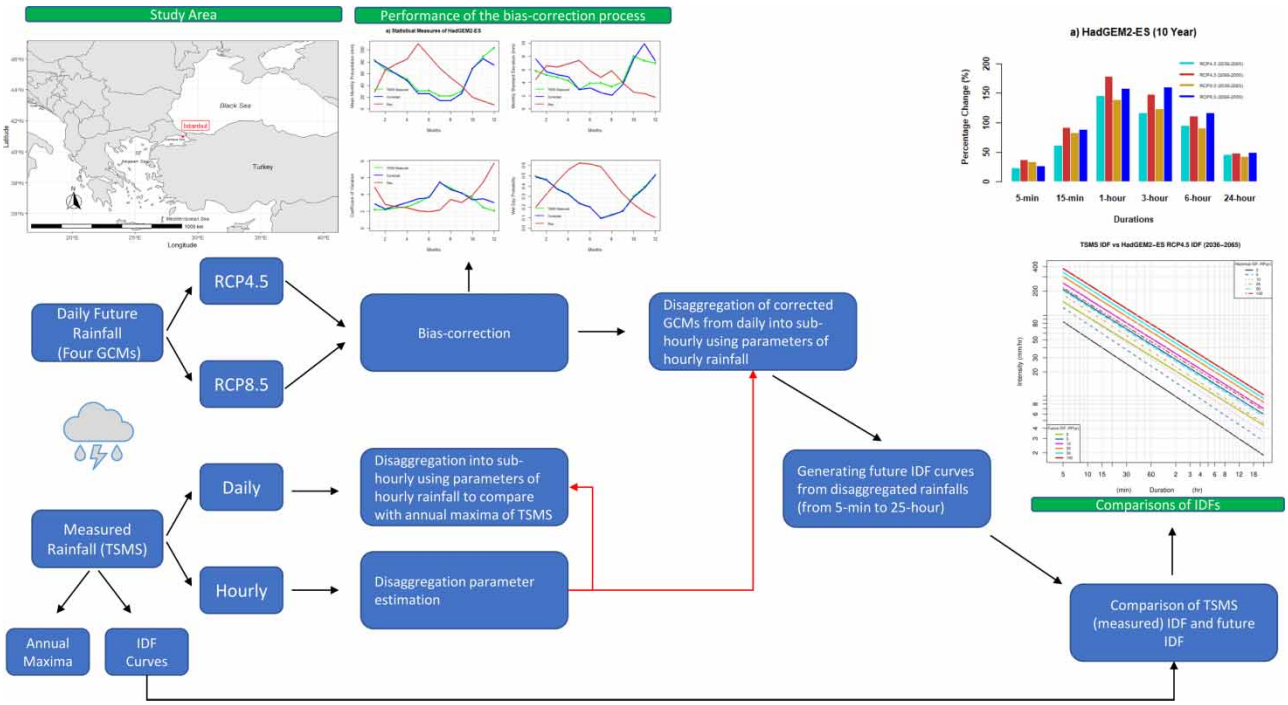
HIGHLIGHTS

- Climate change impacts on rainfall intensities are assessed by comparing historical IDF curves with future IDF curves considering different GCMs and RCPs.
- Short-duration rainfalls under climate change impacts were simulated for the assessment of urban floods.
- Future daily rainfall data can be disaggregated into sub-hourly rainfall with a new approach to HYETOS using disaggregation parameters of hourly measured rainfalls.

This is an Open Access article distributed under the terms of the Creative Commons Attribution Licence (CC BY 4.0), which permits copying, adaptation and redistribution, provided the original work is properly cited (http://creativecommons.org/licenses/by/4.0/).

Downloaded from http://iwaponline.com/jwcc/article-pdf/13/2/684/1013633/jwc0130684.pdf
by guest

GRAPHICAL ABSTRACT



1. INTRODUCTION

Dealing with heavy rainfall events that can cause flooding, loss of life, crops, and properties, is challenging for urban areas. High intensity rainfall is a key factor in the occurrence of flooding events. Urban floods in particular are increasing day after day in many countries. Flash floods are one of the most common flood types that occur in urban areas. Short-duration and high intensity rainfalls are usually responsible for flash floods. These floods have destructive effects on people, cities, drainage, bridges, and the economy. Other factors also cause an increase in the destructiveness of flash floods. The number of impermeable surfaces increases continuously due to urbanization. Hence, drainage systems are becoming ineffective against fast runoffs caused by flash floods, and their response time is decreasing (Hosseinzadehtalaei *et al.* 2020). Water is then flowing through cities due to overflow from drainage systems. Since the mentioned factors are predominantly occurring in urban areas, the effective management and awareness of both urban drainage systems and short-duration rainfalls are significant. As mentioned before, serious management of drainage and short-duration rainfalls is necessary. Rainfall Intensity–Duration–Frequency (IDF) curves play a crucial role in assessing flood risk and quantifying heavy rainfalls. IDF curves are also effective tools in designing and operating urban drainage systems. Hence, IDF curves are required in designing hydraulic structures such as sewers, drainages, gutters, and culverts to cope with floods, because understanding extreme rainfalls and their frequency will help drainage systems against floods. IDF curves give a possible rainfall intensity in selected durations for return periods. Using IDF curves in design water facilities allows engineers to be ready for extreme events, hence possible damage can be decreased (Sarhadi & Soulis 2017). IDF curves are widely applied in many water-related projects, flood forecasting and management, and water management (Cheng & AghaKouchak 2014). In addition, IDF curves help not only drainage systems but also other structures vulnerable to water such as railways and telecommunications networks (Hosseinzadehtalaei *et al.* 2020).

Irrepressible growth of industrial activities, urbanization and population enhances greenhouse gases (carbon dioxide, methane, aerosols, etc.) emissions. This enhancement causes major variations in climate and leads to the necessity to deal with a serious challenge in the future: climate change (Mirhosseini *et al.* 2013). Climate change causes global warming by increasing global temperatures, and this causes enhancement of evapotranspiration and water vapour in the atmosphere, hence more extreme events. Extreme rainfall is one of the most serious consequences of these changes. Extreme rainfall events cause flooding and damage to sewers, drainage systems, bridges, and infrastructure (Singh *et al.* 2016; Sarhadi &

Downloaded from http://iwaponline.com/jwcc/article-pdf/13/2/684/1013633/jwc0130684.pdf
by guest

Soulis 2017). However, current IDF curves assume that extreme rainfall events will not change in the future climate conditions (Cheng & AghaKouchak 2014). Hence, developing advanced IDF curves, which are successful at the representation of both historical and future climate conditions, is a huge necessity. With these types of IDF curves, it will be possible to deal with extreme rainfall events under non-stationary climate conditions. To generate IDF curves, theoretical probability distribution functions such as Gumbel, Generalized Extreme Value (GEV), Log-Normal, and Log Pearson Type III are applied (Nwaogazie *et al.* 2019). Although IDF curves based on historical rainfall events are used frequently, they are still not fully sufficient against a rapidly changing environment. Historical rainfall-based IDF curves are stationary; therefore, they are ineffective in catching climate change conditions (Singh *et al.* 2016). Many studies have been performed to update IDF curves considering future conditions. Mirhosseini *et al.* (2013) evaluated 3-hourly precipitation data generated by six Global Climate Models (GCMs) and Regional Climate Models (RCMs) to examine changes in future IDF curves compared with current ones in Alabama. They performed bias-correction using the quantile-based mapping method. They concluded that rainfalls are expected to be less for short durations (less than 4 h) in the future. Therefore, short-duration rainfalls are serviceable for designing municipal infrastructures. Hajani (2020) generated future stationary and non-stationary IDF curves to compare them with standard regional ARR (Australian Rainfall-Runoff) IDF curves. She also exhibited the impact of climate change on these curves. GEV distribution was applied to arrange the stationarity of the curves by keeping GEV's parameters constant or dependent on time. The study concluded that standard regional IDF curves better match the new stationary IDF curves when compared with non-stationary IDF curves. In the study of Zhu *et al.* (2012), they investigated the generation of IDF curves that were affected by climate change to evaluate rainfall extremes by considering historical and future climate data. Future IDF curves were developed for six locations that represent various climatic conditions in the United States, and the annual maximum series were calculated for 3, 6, 9, 12, 18, 24, 48, and 96 h. An approach called Areal Reduction Factor (ARF) was proposed to relate maximum rainfall intensity measured at a station with the maximum areal average gridded rainfall intensity. They concluded that climate change impacts are more effective at the regional level; hence, evaluations need to be performed locally. Short-duration and high intensity rainfalls are greatly affected by climate change, according to their study. De Souza Costa *et al.* (2020) performed a study on IDF curves using HadGEM2-ES, CanESM2, and MIROC5 models generated under RCP4.5 and RCP8.5 scenarios for the Amazon region, Brazil. They used future daily maximums, measured sub-daily maximums and historical daily maximums. This study concluded that annual rainfalls are decreasing on CanESM2 and HadGEM2-ES models while they are increasing for the MIROC5 model. MIROC5 has the largest difference and CanESM2 has the smallest difference when compared with existing IDF values.

Flash floods are more challenging to deal with compared with slower floods occurring from long-duration rainfalls. Therefore, knowledge of short-duration rainfall (i.e., rainfall durations of less than 4 h) is crucial for the design of urban drainage systems and for urban hydrology studies. Hence, IDF curves must be generated considering short-duration rainfalls for a healthier environment in cities. However, measuring short-duration rainfall is not always possible due to its cost, limitations of a station's capacity, climatic, and geographic conditions. On the other hand, daily rainfalls exist due to its convenience for measurement. It is vital to use some methods to simulate these kinds of rainfalls from longer durations (i.e., daily). In this study, a method called 'disaggregation' was applied to obtain sub-hourly rainfalls.

The main purpose of this study is to generate future rainfall IDF curves using short-duration rainfalls to assess urban floods using an ensemble of four GCMs and then compare them with IDF curves generated by measured rainfalls. Florya meteorological station operated by the Turkish State Meteorological Service (TSMS) in Istanbul was selected as the study area since TSMS provides IDF curves and a wide range of daily measured rainfalls (1980–2005) for the station. In addition, TSMS provides hourly rainfall records for the 14-year period (2005–2018). To assess future rainfall events for the period 2036–2065 and 2066–2095 considering climate change impacts, GCMs generated under Representative Concentration Pathway (RCP) scenarios RCP4.5 and RCP8.5 were provided. Criteria for selecting these periods were as follows: (i) We aimed to evaluate future rainfall intensities for the near future, which is 2036–2065 and for the distant future, which is 2066–2095. Analyses for a wide range are not always a reliable method since there will be significant variations and uncertainty. Therefore, the analyses could mislead the results. Besides, separating years into near and distant futures will help us to take precautions for cities considering the closeness of disasters. (ii) Since four GCMs were used in the study, it was necessary to select common periods for all GCMs. HadGEM2-ES developed by the Met Office Hadley Centre Institute (MOHC), ICHEC-EC-EARTH developed by the Irish Centre for High-End Computing (ICHEC), IPSL-IPSL-CM5A-MR developed by Institut Pierre-Simon Laplace (IPSL), and NorESM1-M developed by Norwegian Climate Center (NCC) were selected as GCMs to generate future IDF curves. When the future conditions are considered, there is a huge uncertainity about variations. Using only one climate model

Downloaded from http://iwaponline.com/jwcc/article-pdf/13/2/684/1013633/jwc0130684.pdf
by guest

can be insufficient to capture changes in rainfall. Hence, more reliable and efficient IDF analyses were intended using an ensemble of GCMs in the study.

In the study, future rainfall intensities (mm/h) from each GCM were computed for selected durations (5, 10, 15, and 30 min; 1, 2, 3, 4, 5, 6, 8, 12, 18, and 24 h) and for each return period of 2, 5, 10, 25, 50, and 100 years. The Gumbel function was selected as the probability distribution function (PDF) for annual maximum rainfall events to generate IDF curves since the past studies reported that the Gumbel distribution is a very effective method to fit annual extreme rainfalls (Oyebande 1982). However, GCMs are not suitable to use directly due to biases between measured and historical raw rainfall data. The distribution mapping method was applied to correct these biases.

As mentioned before, providing short-duration rainfall is challenging due to various factors. Provided future rainfall events were in daily form; hence, a Barlett–Lewis model-based disaggregation model called 'HYETOS' developed by Koutsoyiannis & Onof (2001) was applied for the disaggregation of daily rainfall into sub-hourly to generate IDF curves with short and long durations, which are in the range of 5 min and 24 h. Bartlett–Lewis disaggregation model parameters are required for the disaggregation process and obtained using some statistics of hourly rainfall data. Since future rainfall data is daily, it is not possible to compute HYETOS parameters for future rainfalls. Hence, parameters computed by Florya station's hourly measured rainfalls were used as the disaggregation parameters of future data. Since the disaggregation process is based entirely on rainfall statistics, the most accurate way to conduct the disaggregation process is to use the parameter sets obtained from measured rainfall patterns. In this case, the future rainfalls of Florya station were disaggregated using separately obtained disaggregation parameters for each month from the measured rainfalls in order to perform the most accurate disaggregation. Thus, even if the rainfalls change in the future, the disaggregation can be performed by imitating the past rainfall. All computations, analyses, and plottings were made on the R Studio platform in this study.

This study has six main objectives: (i) Generating more reliable and effective future IDF curves under various climate change scenarios for urban area drainage systems by evaluating short-duration future rainfall data. To date, only a few studies have generated IDF curves for short-duration rainfalls considering climate change. (ii) Disaggregation of future daily rainfalls into sub-hourly rainfalls with a new approach to the HYETOS disaggregation model. Providing sub-hourly rainfall data is not always possible even for simulated rainfalls. Besides, measuring this kind of short-duration data is highly challenging for meteorological stations. HYETOS model usually uses random parameters for the disaggregation process. In this study, disaggregation parameters were obtained from 14-year measured hourly rainfall and parameter sets were determined for each month using some statistical measures. Afterwards, the determined parameters were applied for the disaggregation of measured (applied to test the method) and future daily rainfalls. This process gives a chance for future data to capture historical patterns of a selected region's rainfall instead of random rainfall characteristics during the disaggregation process. Briefly, with this method, it will be possible to disaggregate any daily rainfalls of a large region or city using only short records of hourly rainfall. (iii) To verify the accuracy of the selected disaggregation model by comparing maximum values of disaggregated rainfalls with measured ones. (iv) Applying an effective bias-correction process to GCMs to obtain more reliable future rainfalls. (v) Evaluation of the climate change impact on rainfall intensities by comparing historical and future IDF curves. The IDF curves obtained from the ensemble of four GCMs under RCP4.5 and RCP8.5 scenarios were also compared with each other. (vi) Assessment of climate change impacts on short-duration rainfall using IDF curves. Finally, the study will provide a useful methodology for designing urban drainage systems against floods.

2. WORKFLOW OF THE STUDY

The first step in the process was to estimate disaggregation parameters from hourly measured rainfalls provided by TSMS. As mentioned before, 1-h rainfall is necessary to obtain HYETOS disaggregation parameters. After obtaining parameters, daily measured rainfalls of TSMS were disaggregated into sub-hourly rainfalls (5, 10, 15, and 30 min) using the parameters of hourly rainfalls. Afterwards, the sub-hourly rainfalls were aggregated until 24 h. Maximum rainfalls for each selected duration (5, 10, 15, and 30 min; 1, 2, 3, 4, 5, 6, 8, 12, 18, and 24 h) and for the 1980–2005 periods were supplied by TSMS. Maximum values of rainfalls disaggregated by daily measured rainfall were computed for each selected duration. To verify the accuracy of the disaggregation method, maximum values of both measured and disaggregated rainfalls were then compared. In the next phase of the study, biases of all four GCMs were corrected with the help of TSMS (measured) daily rainfall. Again, the corrected daily GCMs were disaggregated into sub-hourly rainfalls using the previously estimated disaggregation parameters of TSMS hourly measured rainfall. IDF curves for each scenario and each GCM were generated considering all durations (from

Downloaded from http://iwaponline.com/jwcc/article-pdf/13/2/684/1013633/jwc0130684.pdf
by guest

5 min to 24 h) and all return periods (2, 5, 10, 25, 50, and 100 years) using the Gumbel method. Finally, future IDF curves were compared with the IDF curves of measured rainfalls (TSMS IDF) provided by TSMS. Future IDF curves under different GCMs and scenarios were compared with each other to deduce the behaviour of models and scenarios under climate change. Figure 1 summarizes the work done for the study.

3. STUDY AREA

The study area of Istanbul is located in north-western Turkey. The city is located in the Marmara region with a total area of 5,343 km^2 and a population of 15,519,267. The geographical location of the city is 41°00′49″N 28°57′18″E. One of the most important characteristics of this city is that it separates Europe and Asia. Thus, the city has lands in both Europe and Asia. The Black Sea and the Marmara Sea are connected in Bosphorus. Istanbul has the highest population in Turkey and Europe. The hottest months are July and August, with an average temperature of 23.8 °C, and January is the coldest month with an average temperature of 6.0 °C. In the summer months, the average rainfall amount is 106.2 mm, the average rainfall for the other 9 months is 87.7 mm. Istanbul is rainy on average 130 days a year. The average total rainfall per year is 817.4 mm. The wettest month is December with 122.6 mm rainfall and the driest month is July with 31.6 mm. January has the highest number of wet days with 17.5 days, and July has the lowest number of wet days with 4.2 days. The maximum rainfall measured in a day is 227 mm (BBC Weather 2020; TSMS 2020). Rainfall data were provided for Florya meteorological station operated by TSMS in Istanbul. IDF curves and rainfalls in daily and hourly resolution were required for the study. Florya station was selected since the required data are existing. Future climate data obtained from four GCMs were generated for the selected station (Figure 2).

Table 1 includes the station properties and sensor types that W is wind, T is temperature, M is moisture, R is rainfall, ST is soil temperature and P is pressure. Data are collected from Automatic Meteorological Observation Station (AMOS) and daily climate (DC) stations.

4. DATA

4.1. Measured data

TSMS is a meteorological service that provides all kinds of meteorological data. In this study, (i) measured daily rainfall data, (ii) measured hourly rainfall data, (iii) maximum values for the selected durations, and (iv) IDF curves generated under measured rainfalls were provided by TSMS.

The HYETOS parameters are required to have at least 1-h resolution rainfall data to determine disaggregation parameters because they are calculated using the statistics of 1, 6, 12, and 24-h rainfalls. Hourly rainfall data are available for Florya station for the period 2005–2018. These rainfall data were used to obtain disaggregation parameters to be used for the disaggregation of future rainfalls (2036–2095) and daily measured rainfalls (1980–2005). In addition, the maximum values of

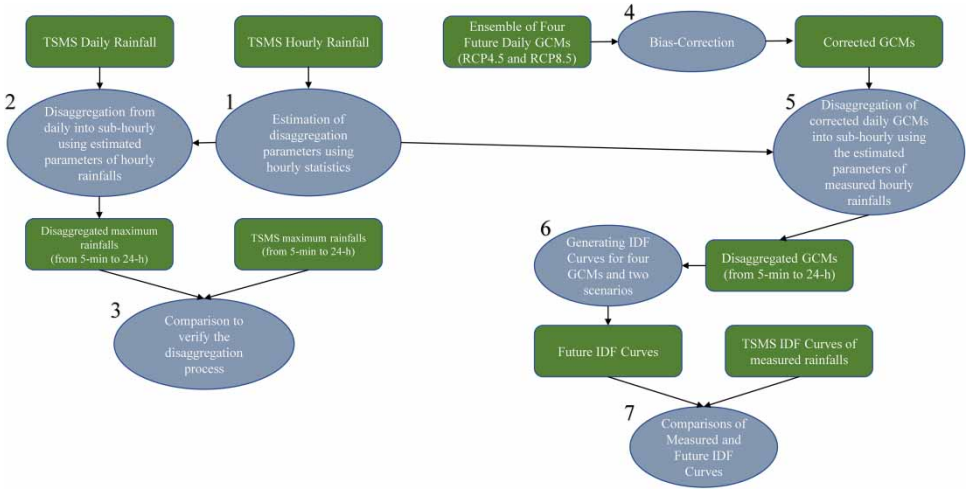


Figure 1 | Workflow of the analyses.

Downloaded from http://iwaponline.com/jwcc/article-pdf/13/2/684/1013633/jwc0130684.pdf
by guest

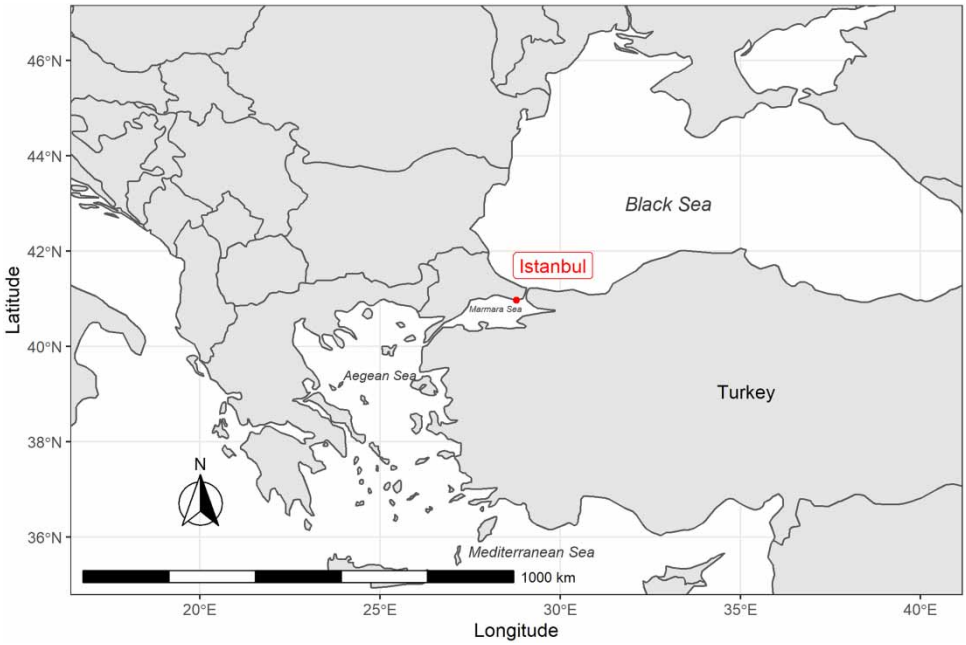


Figure 2 | The location of the selected station in Istanbul.

Table 1 | Station properties

Station	Station number	Coordinates	Sensors	Observation type	Elevation (m)
Florya	17636	40°58′32.9″N 28°47′11.4″E	W, T, M, R, ST, P	AMOS-DC	37

measured rainfalls for each selected duration for the period of 1980–2005 were provided by TSMS. The accuracy of the selected disaggregation method was evaluated by comparing these TSMS maximum rainfalls with maximum rainfalls disaggregated from daily measured rainfalls for each duration. Finally, the IDF curves generated by TSMS using 78 years of rainfall record (1938–2015) were used for the comparisons with future IDF curves for each scenario and GCM.

Monthly rainfall characteristics of Florya station are given in Table 2.

Table 2 | Rainfall characteristics of monthly rainfalls of Florya station

Statistics	January	February	March	April	May	June
Mean (mm)	77.16	73.14	55.6	40.91	28.04	32.24
Min (mm)	0	0	0.2	0	0.4	0.2
Max (mm)	158.4	164.4	117.2	115.2	77	127.6
Standard Deviation (mm)	50.49	52.54	32.75	33.35	21.87	33.69
	July	**August**	**September**	**October**	**November**	**December**
Mean (mm)	19.69	14.31	35.68	63.78	53.51	60.37
Min (mm)	0	0	0	0.2	0	0
Max (mm)	65.4	72	135.6	238	122.8	136.4
Standard Deviation (mm)	23.19	21.08	44.5	62.8	38.07	52.97

Downloaded from http://iwaponline.com/jwcc/article-pdf/13/2/684/1013633/jwc0130684.pdf
by guest

As mentioned in previous sections, GCMs are not available to use directly due to biases between measured and historical raw data. Historical raw data, measured data, and future data were used together for the bias-correction method. As measured data to be used in the bias-correction process, daily rainfalls for the period of 1980–2005 were supplied by the TSMS.

4.2. Global climate model (GCM)

Climate models represent the climate system under various carbon emission scenarios to understand future changes. GCM can be used to simulate both historical and future rainfall events. As mentioned before, dealing with changes in the future using a single GCM is not effective, because each model has advantages and disadvantages, and these disadvantages can create some trouble about capturing rainfalls. Therefore, this study employs an ensemble of four GCMs to provide a more reliable IDF generation. The historical raw and future data were obtained from the Earth System Grid Federation ESGF – Lawrence Livermore National Laboratory (LLNL) website. Daily historical raw rainfalls for the period 1980–2005 were used in the study. Daily future rainfall data are also available for 2036–2065 and 2066–2095 with RCP4.5 and RCP8.5 scenarios for selected GCMs. As mentioned before, separating future into the near and distant future will give more reliable results, because the selection of a wide range period for analyses will lead to significant variations. In addition, the selected periods were common for all GCMs. GCMs were provided from the Coordinated Regional Climate Downscaling Experiment (CORDEX) Europe program. GCMs HadGEM2-ES, ICHEC-EC-EARTH, IPSL-IPSL-CM5A-MR, and NorESM1-M with a 12.5 km (0.11°×0.11°) resolution were preferred in this study. The reason for selecting these GCMs was their availability for the desired factors (the presence of both RCP4.5 and RCP8.5 scenarios, Europe domain, and 12.5 grid resolution). Outputs from the GCMs were downscaled to Florya station in this study. To correct the biases between measured and historical raw data, the bias-correction method distribution mapping was employed.

The Intergovernmental Panel on Climate Change (IPCC) published the Fifth Assessment Report (IPCC 2014) to assess climate change in the future using RCP scenarios. RCPs are used to define emissions of air pollutants, greenhouse gases, and atmospheric concentrations. Radiative forcing is 4.5 W/m^2 for RCP4.5 and 8.5 W/m^2 for RCP8.5. These values are valid on a global scale, and they give approximate total radiative forcing for each RCP scenario in 2100 (Edenhofer *et al.* 2015). Watts per square meter (W/m^2) is the unit of solar radiation falling per unit area. It also represents the energy imbalance in the atmosphere. Table 3 shows each GCM and RCM, centre of models, resolutions, and scenarios, respectively. Figure 3 presents all the data types used in the study with their periods.

5. METHODS

5.1. GCM data bias-correction

GCM outputs are not suitable for direct use in hydrological studies due to the need for bias-correction. These biases originate from inconsistencies between measured and historical raw rainfall (Rathjens *et al.* 2016). Measured high rainfalls and the number of dry days cannot be well-represented if biases exist. Seasonal alterations and extreme temperatures are predicted poorly due to biases. GCMs simulate low rainfall days instead of dry days (Teutschbein & Seibert 2010). The Climate Model Data for Hydrologic Modeling (CMhyd) software developed by Texas A&M University (TAMU) which is available online was chosen as a bias-correction process. The general framework of the bias-correction process was described by Rathjens *et al.* (2016) as shown in Figure 4. First, biases between measured rainfall and historical raw climate data are

Table 3 | Description of selected climate models

Driving GCM	RCM	GCM Model centre	RCM Model centre	Resolution	Scenario
HadGEM2-ES	CCLM4-8-17	Met Office Hadley Centre	The Climate Limited-area Modeling Community	0.11°× 0.11°	Historical, RCP4.5 and RCP8.5
ICHEC-EC-EARTH	KNMI-RACMO22E	Irish Centre for High-End Computing	Royal Netherlands Meteorological Institute	0.11°× 0.11°	Historical, RCP4.5 and RCP8.5
IPSL-IPSL-CM5A-MR	IPSL-WRF381P	Institut Pierre-Simon Laplace	Institut Pierre-Simon Laplace	0.11°× 0.11°	Historical, RCP4.5 and RCP8.5
NorESM1-M	GERICS-REMO2015	Norwegian Climate Center	Climate Service Center Germany	0.11°× 0.11°	Historical, RCP4.5 and RCP8.5

Downloaded from http://iwaponline.com/jwcc/article-pdf/13/2/684/1013633/jwc0130684.pdf
by guest

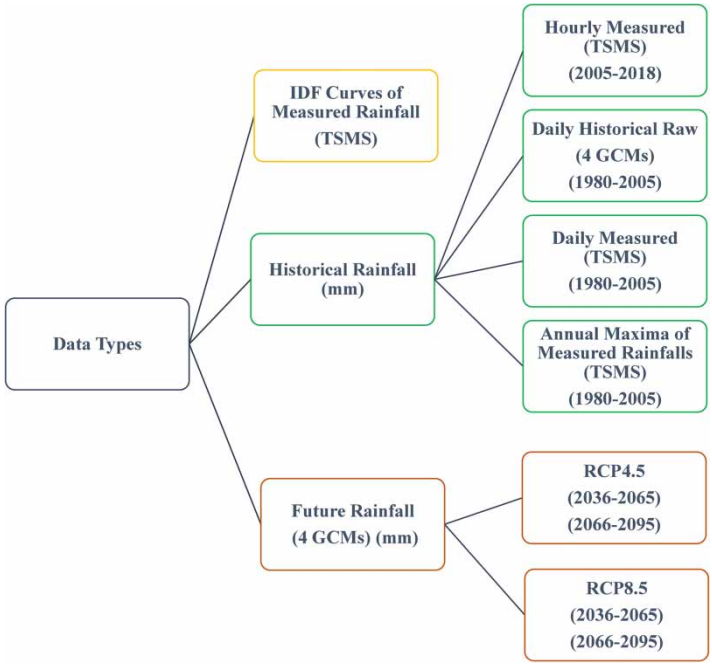


Figure 3 | Used data types.

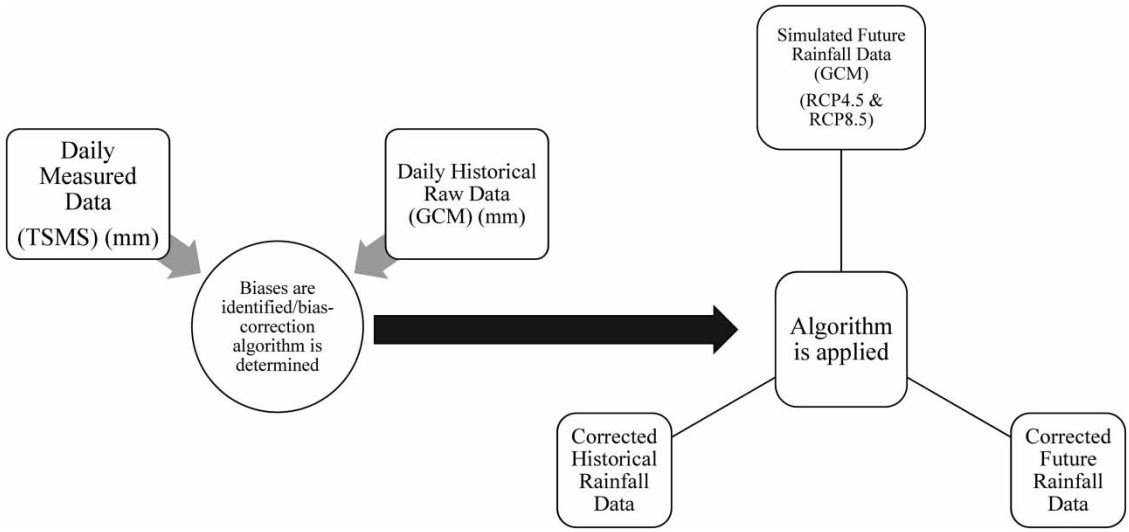


Figure 4 | Framework of bias-correction.

identified, and the parameters of bias-correction algorithm are then determined. This algorithm is then applied to future climate data to correct biases. This way, one can finally obtain corrected historical and future climate data. Bias-correction helps users to use GCMs in hydrological studies by bringing simulated data closer to real data. Several bias-correction methods, including distribution mapping, were explained in the study of Teutschbein & Seibert (2010). In this study, the distribution mapping method was employed as the bias-correction method and biases between overlapping periods of measured and historical raw rainfalls were corrected.

Measured TSMS data and GCM historical raw data between 1980 and 2005 were used as the calibration period for the bias-correction process.

Downloaded from http://iwaponline.com/jwcc/article-pdf/13/2/684/1013633/jwc0130684.pdf
by guest

5.1.1. Distribution mapping

Teutschbein & Seibert (2010) applied this method in their studies. 'Probability mapping', 'quantile matching', 'statistical downscaling', and 'histogram equalization' terms can be used for distribution mapping in the literature. Using distribution mapping, the distribution function of simulated climate data is corrected to coordinate the measured data distribution function. To perform this analysis, a transfer function is used to shift the distribution of simulated data. It is assumed that the biases are stationary under climate change for this method (Teutschbein & Seibert 2010). Distribution mapping employs the Gamma distribution to remove biases. Thom (1958) expressed the Gamma distribution with shape parameter k, and scale parameter β. The Gamma distribution is applicable to the distribution of rainfall data (Teutscbein & Seibert 2010).

$$f_y = \frac{1}{\beta^k \Gamma(k)} x^{k-1} e^{-x/\beta};\ x \geq 0;\ \beta, k > 0 \tag{1}$$

where β is the scale parameter, k is the shape parameter, Γ is the gamma function, and x is the normalized daily rainfall. Each grid and month has its own scale and shape parameter. With this method, mean, variance, skew, and frequency of rainfall events are corrected. The distribution profile is managed by shape parameter k. Three conditions are considered for the value of k. When $k < 1$, it defines the exponentially shaped Gamma distribution, $k = 1$ describes the exponential distribution, and $k > 1$ indicates a skewed uni-modal distribution. The scale parameter β dictates dispersion of the Gamma distribution. Commonly $k > 1$ situation is used for measured daily rainfall. If the scale parameter β is small, it eventuates to a more compressed distribution, and this ends up with lower probabilities of extreme rainfall. If the β is large, this causes a stretched distribution, and this is the reason for higher probabilities of extreme events (Teutscbein & Seibert 2010). The study by Teutschbein & Seibert (2010) showed that gamma distribution parameters fitted to simulated climate data show similar patterns for the selected catchments in the study area. They reported that the level of commitment of the distribution parameters (k/β) defines the skill for the GCM to reproduce rainfall. As mentioned before, Teutschbein & Seibert (2010) compared several bias-correction methods including linear scaling, local intensity scaling, power transformation, variance scaling, and distribution mapping considering the skills of methods to arrange the statistics of the respective measured climate data. The study concluded that distribution mapping is the best method for rainfall with the minimum MAE (minimum absolute error). They also concluded that the method is applicable to both current and future climate data.

5.2. Disaggregation of daily rainfalls into sub-hourly rainfalls

Hydrological studies such as designing drainage systems require high-resolution rainfall data for the generation of IDF curves. This need arises from the fact that maximum values of finer scales of rainfall are responsible for urban floods. However, providing sub-hourly rainfall data is not always possible even for simulated rainfalls. Besides, measuring this kind of short-duration data is highly challenging for meteorological stations due to the limitations of a station's capability, costs, and geographic conditions. To cope with this shortcoming of sub-hourly data, disaggregation methods, which are able to calculate finer-scale data (i.e., hourly and sub-hourly) from coarser-scales (i.e., daily data), are used. In this study, we intend to generate future IDF curves for short and long durations ranging from 5 min to 24 h. Hence, the disaggregation process was used to disaggregate GCMs into sub-hourly rainfalls.

Koutsoyiannis & Onof (2001) developed a computer programme called HYETOS based on the Bartlett–Lewis model, and they implemented a disaggregation scheme in an R package called 'HYETOSMinute'. The Bartlett–Lewis model was constructed by Rodriguez-Iturbe *et al.* (1987) to overcome the inefficiency of simple Poisson models. In this study, the HYETOS disaggregation model was applied.

The original Bartlett–Lewis model has five parameters (β, γ, μ_x, η, and λ) for the disaggregation process. Storm origins are developed by λ, cell origins are developed by β, cell arrivals end after a specific time, and the time is exponentially distributed with γ. Each cell has a duration exponentially distributed with η. Uniform intensity for each cell is distributed exponentially with μ_x. Hanaish *et al.* (2011) explained the original Bartlett–Lewis rectangular pulses model in their study.

Rodriguez-Iturbe *et al.* (1988) adjusted the original model to boost the flexibility of the model to generate larger diversity of rainfall. This modified model is called the Modified Bartlett–Lewis Rectangular Pulse Model (MBLRPM). With the Gamma distribution, η varies for each storm.

In this model, β and γ also altered, therefore ratios $k{=}\beta/n$ and $\varphi{=}\gamma/\eta$ stay constant, so that the MBLRPM model has six parameters (α, φ, μ_x, k, λ, v). An enhanced version of the Evolutionary Annealing-Simplex Method (EAS) is applied to

Downloaded from http://iwaponline.com/jwcc/article-pdf/13/2/684/1013633/jwc0130684.pdf
by guest

estimate Bartlett–Lewis model parameters. Four historical statistical values (mean, variance, auto-covariance lag-1, and the proportion of dry days) for 1-, 6-, 12-, and 24-h time scales of rainfall data are used to make the estimation. MBLRPM parameters are used as inputs to the disaggregation method. Each month also has its own parameters for the disaggregation process. Bartlett–Lewis parameters cannot be calculated for future data due to the absence of hourly future rainfall data. In this study, six different disaggregation parameters were obtained from rainfall statistics for each month of 14 years (2005–2018). Afterwards, mean values of parameters were computed, and histograms were plotted for parameter values of 12 months, separately. Twelve different parameter sets were determined for each month with the help of histogram plots and mean values. For instance, 12 parameter sets containing six parameters (α, φ, μ_x, k, λ, v) were determined for each month. Each parameter reflects the dominant rainfall characteristics of each month. Thus, each GCM has parameters for the disaggregation of future rainfall data. Afterwards, the determined parameters were applied for the disaggregation of respective months of measured (applied to test the method) and future daily rainfalls.

For the assessment of accuracy of the selected disaggregation method HYETOS, daily measured rainfalls provided by TSMS were disaggregated using disaggregation parameters of hourly rainfalls. Since IDF curves are generated with annual maximums of each duration, maximum values of disaggregated rainfalls were computed for each selected duration. Therefore, evaluating the relationship of maximum values was sufficient to deduce the performance of the disaggregation method. A comparison was made between the maximum rainfalls of TSMS and the maximum of disaggregated rainfalls. Results showed that maximum values of disaggregated and measured rainfalls are in good agreement with each other. This shows that the MBLRPM can be used as a disaggregation method.

5.3. Generating future IDF curves

IDF curves represent a relationship between rainfall intensity and storm duration for given return periods (T). Each IDF curve value shows the probability of occurring on average $1/T$ for each year. For example, if an IDF curve value is calculated for a 100-year return period and a 6-h duration, this extreme rainfall value can occur in any given year with 1/100 (% 1) chance. Periods of 2, 5, 10, 25, 50, and 100 years were selected as a return period, and 5, 10, 15, 30 min, 1, 2, 3, 4, 5, 6, 8, 12, 18, and 24 h were used as standard durations.

The GCMs generated under RCP4.5 and RCP8.5 climate change scenarios were used to generate future IDF. In determining future IDF curves, the annual maximum rainfall values for each standard duration for both the near future and distant future (2036–2065 and 2066–2095) are required. In this study, future IDF curves of GCMs HadGEM2-ES, ICHEC-EC-EARTH, IPSL-IPSL-CM5A-MR and NorESM1-M under two climate change scenarios RCP4.5 and RCP8.5 for two selected periods 2036–2065 and 2066–2095 were generated. Finally, 16 different IDF tables were generated to be compared with each other to present (i) climate change impact on rainfall intensities, (ii) differences between GCMs and RCP scenarios, and (iii) behaviour of short- and long-duration rainfalls under climate change.

PDFs are used to generate IDF curves. Generally, the Gumbel probability distribution function is used for the determination of IDF curves. Oyebande (1982) reported that the Gumbel distribution is a very effective method to fit annual extreme rainfalls. Other extreme value distributions such as Frechet and Weibull distributions require three parameters: location, scale, and shape. When the shape parameter is set to zero, they transform to Gumbel. Therefore, Gumbel has only two parameters: location and scale. The function of Gumbel PDF is defined as:

$$F(x) = \frac{1}{\beta} e^{\frac{x-\alpha}{\beta}} e^{-e^{\frac{x-\alpha}{\beta}}} \tag{2}$$

where α is the location, and β is the scale parameter. In this study, Method of Moments (MoM) was applied for the estimation of distribution parameters. Calculating rainfall intensities requires a Gumbel frequency factor for each return period. The mean and standard deviation of annual maximum values for each duration are then calculated. The Gumbel frequency factor K_T is calculated using the following equation (Nwaogazie *et al.* 2019):

$$K_T = \frac{\sqrt{6}}{\pi}\left[0.5772 + \ln\left[\ln\left[\frac{T}{T-1}\right]\right]\right] \tag{3}$$

where T is the return period.

Downloaded from http://iwaponline.com/jwcc/article-pdf/13/2/684/1013633/jwc0130684.pdf
by guest

The value of random variable R, which is rainfall (mm) for this study, was found with the equation given by Chow (1951):

$$R = M + K_T S \tag{4}$$

where R is rainfall (mm), M and S are the mean and standard deviation of measured maximum rainfall for the current duration, respectively, and K_T is the Gumbel frequency factor for each return period. Hence, rainfall values are calculated for the current duration at different return periods. Rainfall intensity I (mm/h) can be calculated by dividing rainfall R by selected duration d (in hours).

$$I = \frac{R}{d} \tag{5}$$

Then, the process is performed for each duration, and maximum rainfall intensities are obtained for each duration and return period.

Briefly, the steps to generate IDF curves can be given as follows:

1. Annual maximum values of rainfall data for each standard duration (5, 10, 15, and 30 min, and 1, 2, 3, 4, 5, 6, 8, 12, 18, and 24 h) and periods (2036–2065 and 2066–2095) are calculated.
2. MoM is applied to obtain Gumbel parameters.
3. Gumbel frequency factors are determined for each return period.
4. Mean and standard deviation of measured maximum rainfall values are calculated for each duration.
5. Rainfall values are obtained following Equation (4) and rainfall intensity is calculated by dividing rainfall amounts by durations.
6. The process is repeated for each duration.
7. IDF curves are plotted with calculated rainfall intensities for each duration and return period.

6. RESULTS AND DISCUSSION

6.1. Evaluation of the bias-correction process

The distribution mapping method was applied to correct biases between measured and historical raw data. For the process, measured and historical raw data for periods 1980–2005 were imported for calibration. To evaluate the performance of the bias-correction method, different statistics and plots were used. Root mean square error (RMSE), Nash–Sutcliffe efficiency (NSE) (Nash & Sutcliffe 1970) and the percent bias (PBIAS) were used to test variation between measured rainfalls, raw, and corrected GCM. RMSE measures the estimation error. NSE is an efficient measure to reveal the matching level between measured and simulated. The optimal value for the NSE is 1, which indicates a perfect fit. The average trend of simulated data to measured data can be found by PBIAS. Obtaining negative values from PBIAS shows an overestimation; otherwise, positive values indicate an underestimation. 0 is the optimal value for PBIAS (Berhanu *et al.* 2016). Monthly statistical values, including maximum, mean, median, standard deviation (SD), coefficient of variation (CV), 90th (Q) percentile, and wet day probability (WDP), were calculated as summarized in Table 4 to conduct comparisons.

Afterwards, cumulative distribution functions (CDFs) of all concerned data for May are plotted in Figure 5.

Mean monthly rainfalls, coefficient of variations, standard deviations, and wet day probabilities for each month of measured, raw, and corrected were plotted separately for each GCM (Figure 6). Briefly, using several techniques, measured, historical raw and historical corrected rainfall data were compared to prove the convenience of the selected bias-correction method.

Table 4 shows several statistical measures and tests between measured, raw, and corrected data. When monthly mean rainfalls were compared, there were wide differences between raw and measured data for all GCMs, while corrected data presented closer relationships. All raw data of GCMs underestimate mean monthly rainfalls except IPSL-IPSL-CM5A-MR. As can be seen from the NSE column in Table 4, all corrected GCM data have a highly strong relationship with measured data in the range of 0.87 and 0.98. Raw data of GCMs show NSE values far than 1; however, raw data of NorESM1-M have the strongest relationship with NSE=0.8 when compared with other raw data. Similarly, in RMSE comparisons, there are significant differences for all raw data of GCMs compared with corrected data. Negative PBIAS values indicate

Downloaded from http://iwaponline.com/jwcc/article-pdf/13/2/684/1013633/jwc0130684.pdf
by guest

Table 4 | Mean monthly statistical values and tests of measured, historical raw and corrected data

GCMs and Scenarios	Maximum (mm)	Median (mm)	Mean (mm)	SD (mm)	CV	90th *Q* (mm)	WDP	RMSE (mm)	NSE	PBIAS (%)
Measured	147.00	46.61	54.75	5.07	3.23	5.32	0.31			
HadGEM2-ES Raw	119.32	40.85	45.62	4.91	3.54	5.36	0.38	54.05	−3.0	0.4
HadGEM2-ES Corrected	187.60	29.18	49.69	5.23	3.52	3.46	0.30	9.48	0.87	−9.3
ICHEC-EC-EARTH Raw	93.06	37.40	40.25	3.84	3.10	4.82	0.65	14.39	0.70	−13.9
ICHEC-EC-EARTH Corrected	149.30	51.43	42.44	4.82	3.27	4.81	0.31	3.72	0.98	−5.90
IPSL-CM5A-MR Raw	117.07	57.38	60.77	4.47	2.61	6.98	0.50	25.89	0.03	30.20
IPSL-CM5A-MR Corrected	149.71	45.78	50.39	4.78	3.24	4.44	0.31	4.48	0.97	−7.90
NorESM1-M Raw	110.36	34.60	39.00	4.37	3.83	4.49	0.56	11.39	0.81	−16.4
NorESM1-M Corrected	134.41	50.85	52.55	4.84	3.27	5.02	0.31	4.32	0.97	−3.90

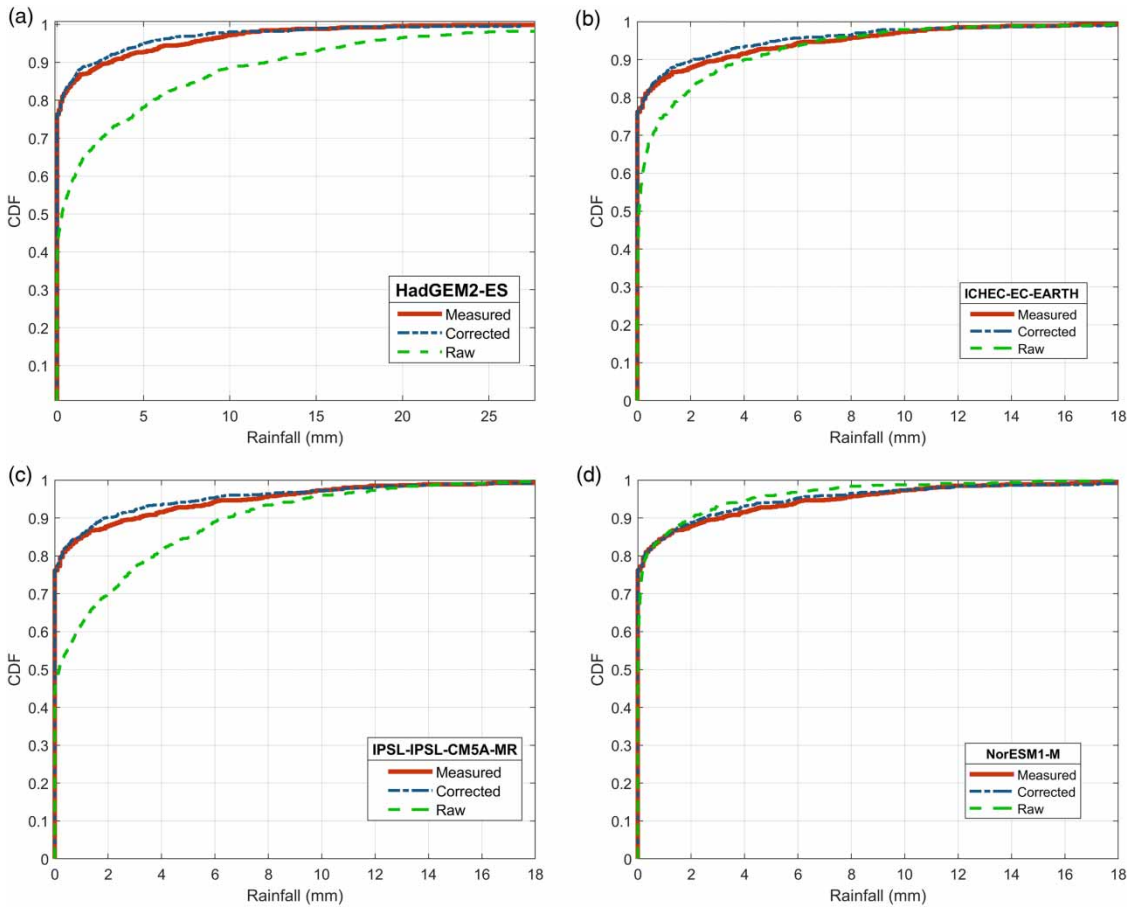


Figure 5 | CDF plots for measured, historical raw, and corrected data for May of (a) HadGEM2-ES, (b) ICHEC-EC-EARTH, (c) IPSL-IPSL-CM5A-MR, and (d) NorESM1-M.

an overestimation of measured data. What stands out in Table 4 is the corrected data of GCMs overestimate measured data, however, all corrected data estimate better than raw data except HadGEM2-ES. The most surprising aspect of the PBIAS values is that raw data from HadGEM2-ES have a closer value to zero. This can be considered surprising since all test values and statistical measures of HadGEM2-ES corrected data are in highly strong relationships with measured data except PBIAS. Figure 5 shows the CDFs of each GCM for May. According to CDF plots, all corrected data are in close relationship with measured data. Figure 6 reveals the variations of raw and corrected data compared with measured data

Downloaded from http://iwaponline.com/jwcc/article-pdf/13/2/684/1013633/jwc0130684.pdf
by guest

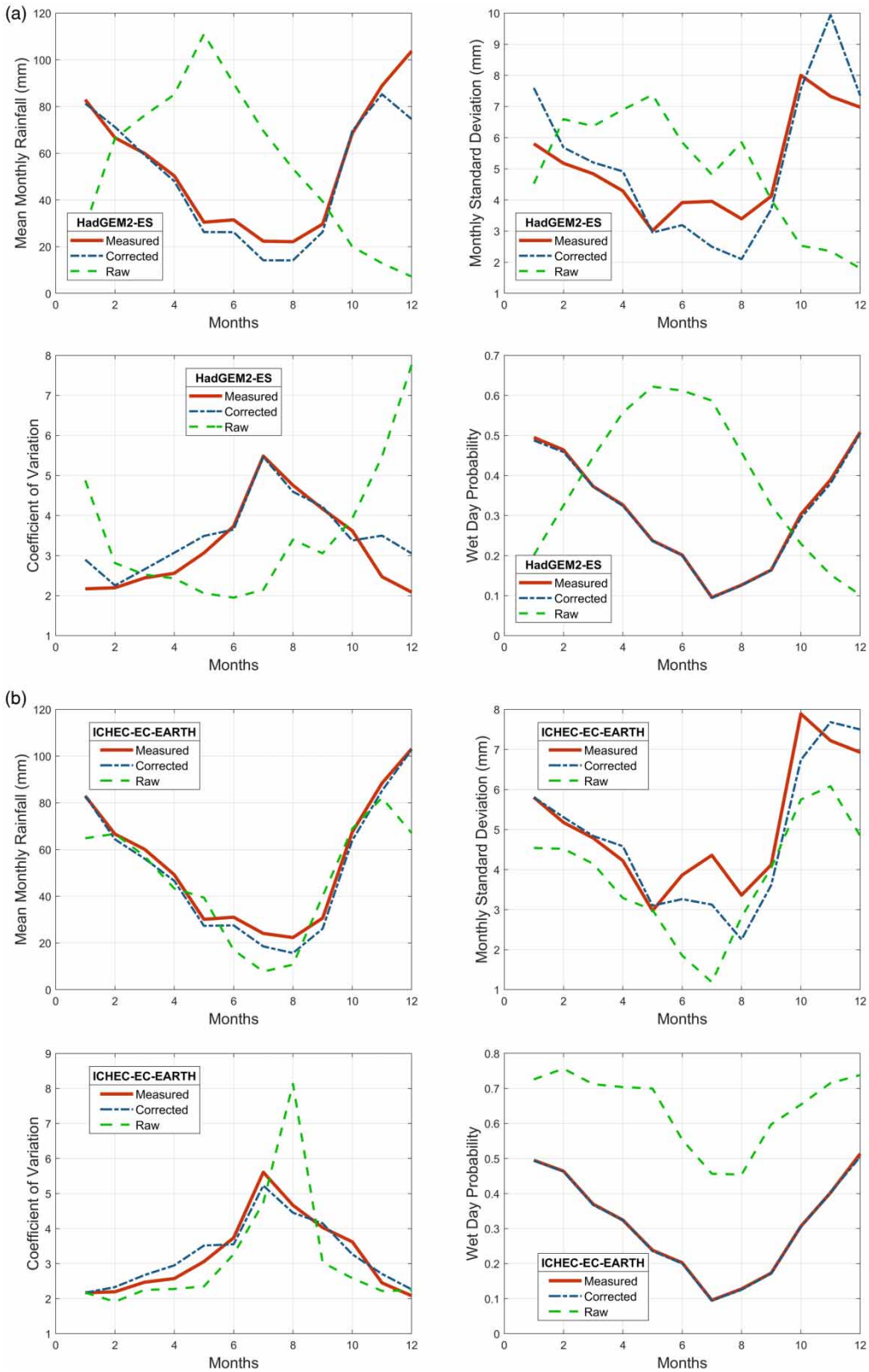


Figure 6 | Plots of monthly statistical measures of each GCM (a) HadGEM2-ES, (b) ICHEC-EC-EARTH, (c) IPSL-IPSL-CM5A-MR, and (d) NorESM1-M (*Continued*).

Downloaded from http://iwaponline.com/jwcc/article-pdf/13/2/684/1013633/jwc0130684.pdf
by guest

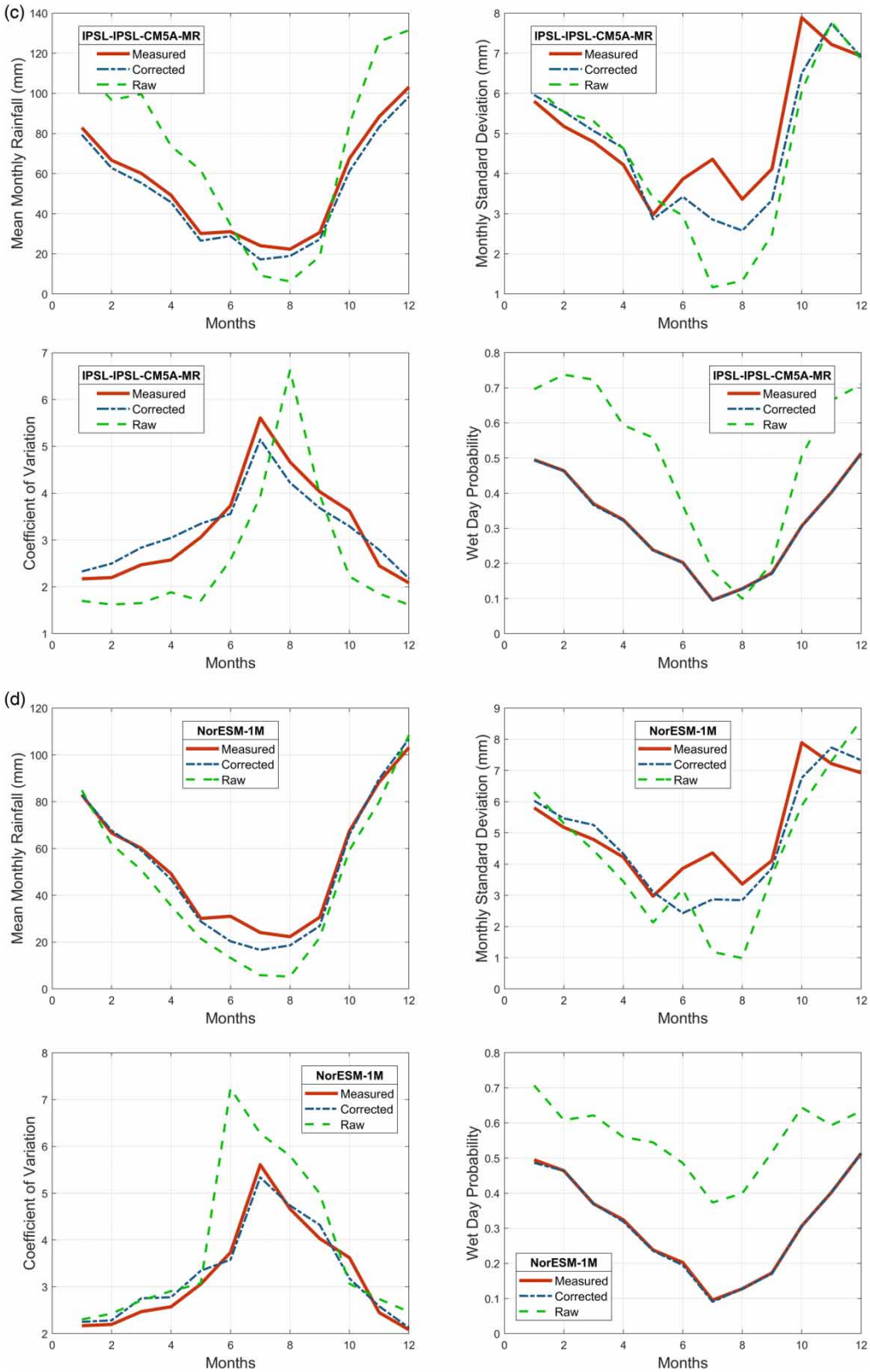


Figure 6 | (Continued.).

Downloaded from http://iwaponline.com/jwcc/article-pdf/13/2/684/1013633/jwc0130684.pdf
by guest

by plotting the statistical measures. As mentioned before, as we can see from the first chart of each GCM, mean monthly rainfalls of raw data show a very weak relationship to measured data. In a similar manner, SDs and CVs for corrected data show a better representation of measured data. As is very clear from WDP charts, corrected and measured have almost the same tendency, while raw data often overestimates wet days. Results conclude that the corrected data of HadGEM2-ES give the worst results compared with others. Even though the corrected data of the other three GCMs show a strong relationship with NSE ranging between 0.97 and 0.98, it is difficult to select the best one between them since they exhibit close values.

The findings of bias-correction analyses have shown that all GCMs show a tremendous representation of measured data when considered substantial measures and tests such as NSE, RMSE, PBIAS, mean monthly rainfalls and other statistics. Briefly, mean, standard deviation, and coefficient of variations were adjusted for almost all months thanks to distribution mapping. It can be said that GCM raw data are improved, and biases are corrected between measured and historical raw data. These results prove that distribution mapping is an effective method for bias-correction. Therefore, future GCMs can be used without any doubt to generate future IDF curves.

6.2. Performance of the disaggregation model

Before applying the disaggregation process for future GCMs, it is necessary to test the performance of the disaggregation model. Since IDF curves are generated using annual maxima for each duration, capturing great correlation between maximum values of measured and disaggregated rainfalls is sufficient for verification. Therefore, in this section, comparisons between maximum values of disaggregated and measured values were performed. Annual maximum rainfalls for each duration for the period of 1980–2005 were provided by TSMS. TSMS daily measured rainfalls (1980–2005) were disaggregated into sub-hourly rainfalls (5, 10, 15, and 30 min) using disaggregation parameters obtained from statistics of hourly rainfalls. Afterwards, these sub-hourly rainfalls were aggregated to longer durations (1, 2, 3, 4, 5, 6, 8, 12, 18, and 24 h). After that, scatter diagrams containing all maximum values of measured and disaggregated rainfalls are plotted in Figure 7. Correlation coefficients between the maxima of disaggregated rainfall and measured rainfall were found at 0.82. The range of correlation coefficients is between -1 and $+1$. A correlation coefficient higher than 0.8 indicates a fairly strong relationship. These comparisons revealed that there is a high correlation between measured and disaggregated rainfall intensities. Since the selected disaggregation model shows a good performance to obtain sub-hourly data from daily data, the process was applied for the disaggregation of daily future rainfall data, as well. The trend of IDF curves generated by TSMS using measured rainfall, and the trend of IDF curves generated by disaggregated rainfalls are plotted together in Figure 8.

6.3. Changes in rainfall intensities under future climate conditions

IDF curves were generated using the Gumbel distribution for selected return periods and durations for an ensemble of four GCMs using the methodology explained in 'Generating Future IDF Curves'. HadGEM2-ES, ICHEC-EC-EARTH, IPSL-IPSL-

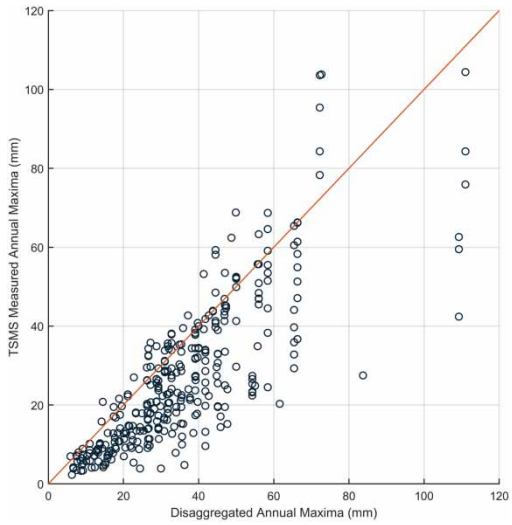


Figure 7 | Scatter plot of annual maxima of disaggregated and measured rainfalls for years 1980-2005.

Downloaded from http://iwaponline.com/jwcc/article-pdf/13/2/684/1013633/jwc0130684.pdf
by guest

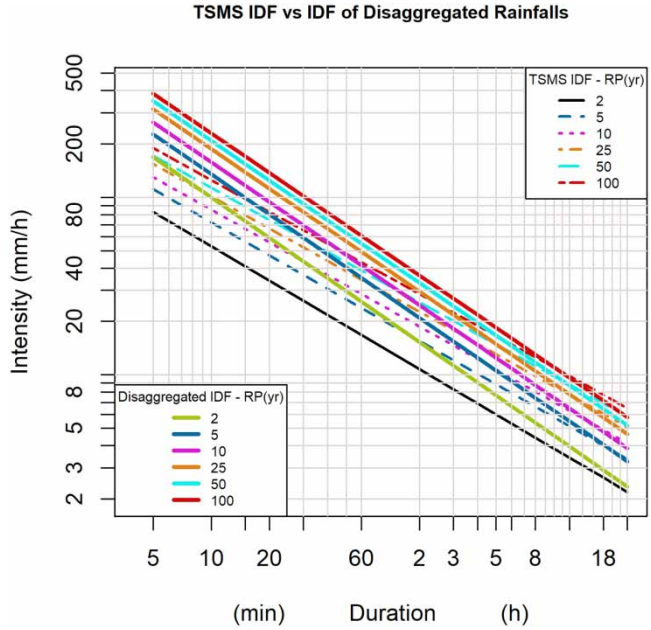


Figure 8 | IDF curve trends of TSMS and disaggregated rainfalls.

CM5A-MR, and NorESM1-M models were preferred. This section deals with the variations of future IDF curves of the near future (2036–2065) and distant future (2066–2095) with respect to TSMS IDF curves (generated by TSMS using measured rainfalls of 1938–2015). Besides, differences between different GCMs and RCP scenarios were exhibited. RCP4.5 and RCP8.5 scenarios were employed to generate GCM. IDF values of measured rainfalls (TSMS) for Florya station are given in Table 5.

In total, 16 different future IDF tables were generated for Florya station (four GCMs, two RCPs, and two future periods). IDF curves were generated for all return periods mentioned before. However, to increase the simplicity of understanding of

Table 5 | TSMS IDF values of Florya Station

Rainfall intensities (mm/h)

	Return periods					
Durations	**2-year**	**5-year**	**10-year**	**25-year**	**50-year**	**100-year**
5 min	73	107	127	151	168	183
10 min	52	77	95	116	131	146
15 min	42	63	76	93	105	117
30 min	28	42	51	64	73	83
1 h	17	25	31	38	44	49
2 h	10	15	19	24	27	31
3 h	8	11	14	18	21	25
4 h	6	9	12	15	18	20
5 h	5	8	10	13	16	18
6 h	5	7	9	12	14	16
8 h	4	6	7	9	11	13
12 h	3	4	5	7	8	10
18 h	2	3	4	5	6	8
24 h	2	3	3	4	5	6

Downloaded from http://iwaponline.com/jwcc/article-pdf/13/2/684/1013633/jwc0130684.pdf
by guest

analyses, tables and figures were shown for a small return period (10 years) and a longer return period (100 years). The first findings of the analyses are summarized in Table 6 for both periods of 2036–2065 and 2066–2095. Table 6 includes average percentage changes in the future IDF values of each GCM and RCP compared with TSMS IDF curves for 10-year and 100-year return periods.

As seen in Table 6, future rainfall intensities tend to increase for all return periods except the 100-year return period of NorESM1-M under RCP8.5 for 2036–2065, and 100-year return period for ICHEC-EC-EARTH under RCP4.5 for 2066–2095. The relative change of the 10-year return period ranges between 17 and 88.6%; changes range between −1.7 and 66.7% for the 100-year return period for 2036–2065. For 2066–2095, 10-year changes range between 7.3 and 106.2%, while 100-year ranges between −11.6 and 61.4%. HadGEM2-ES shows the highest increase for both future periods and for both return periods. Under RCP8.5 scenarios of HadGEM2-ES, rainfall intensities show slight increases compared with RCP4.5 except 10-year for 2066–2095. The 100-year return period of the ICHEC-EC-EARTH RCP4.5 scenario shows the highest decline. For small periods (10-year) return periods, the increase in future rainfall intensities is higher than longer periods (100-year). 10-year intensities tend to increase more for the distant future (2066–2095) than the near future (2036–2065). Most of the RCP8.5 scenarios show a higher increase compared with RCP4.5. This also supports the previous findings in the literature (Xin *et al.* 2013; Nasim *et al.* 2018). However, for some GCMs and return periods, it is possible to see higher intensities under RCP4.5 compared with RCP8.5 as in the study of Singh *et al.* (2016). Similarly, most of the future rainfalls are increasing compared with measured ones; however, there are reductions for several periods in rainfall intensities in the future. A possible explanation for this might be that some GCMs can underestimate rainfalls due to various factors such as diversity of climatic conditions of different regions in the world and uncorrected biases as mentioned in the study of Mirhosseini *et al.* (2013).

Tables 7 and 8 show the average percentage changes in rainfall intensities for both 10-year and 100-year return periods for all GCMs and RCPs compared with measured values in terms of short- and long-duration rainfall intensities for the first future period (2036–2065) and the second future period (2066–2095), respectively. Short-duration rainfall indicates rainfall durations of less than 4 h, and long durations indicate rainfall durations 4 h and longer than 4 h as is suggested in the study by Mirhosseini *et al.* (2013). It is apparent from Tables 6 and 7 that short-duration rainfalls have a rising tendency for all return periods and GCMs in both the near and distant futures. As mentioned before, HadGEM2-ES scenarios have the highest increase compared with other GCMs for both short and long durations for the two return periods. The highest increase in the near future is in HadGEM2-ES under the RCP8.5 scenario with 96.06% and is HadGEM2-ES under RCP4.5 with 116.76% for the distant future. For 2036–2065, IPSL-IPSL-CM5A-MR RCP4.5 has the lowest increase with 29.12% for 10-year short-duration rainfalls, while it is ICHEC-EC-EARTH under the RCP4.5 scenario with 17.31% for 2066–2095. For the 100-year return period in 2036–2065, IPSL-IPSL-CM5A-MR RCP4.5 has the lowest increase with 16.27%. For the 100-year return period, ICHEC-EC-EARTH RCP4.5 is increasing less than other GCMs and RCPs with 5.11% for

Table 6 | Average percentage changes of future IDF values (mm/h) compared with TSMS IDF (mm/h) values for 10-year and 100-year return periods for future periods (2036–2065) and (2066–2095)

Percentage change in rainfall intensities (%)

	(2036–2065) (%)		(2066–2095) (%)	
	Return periods		Return periods	
GCMs and Scenarios	10-year	100-year	10-year	100-year
HadGEM2-ES RCP4.5	88.3	66.3	106.2	61.4
HadGEM2-ES RCP8.5	88.6	66.7	105.8	65
ICHEC-EC-EARTH RCP4.5	25.4	9.9	7.3	−11.6
ICHEC-EC-EARTH RCP8.5	24.1	7.6	27.8	10.7
IPSL-IPSL-CM5A-MR RCP4.5	19.9	1.3	30.9	14.1
IPSL-IPSL-CM5A-MR RCP8.5	28.9	12.4	31.4	12.7
NorESM-1M RCP4.5	25.1	10.3	26.5	7.5
NorESM-1M RCP8.5	17	−1.7	31	9.7

Downloaded from http://iwaponline.com/jwcc/article-pdf/13/2/684/1013633/jwc0130684.pdf
by guest

Table 7 | Average percentage changes of future IDF values (mm/h) compared with TSMS IDF values (mm/h) in terms of short-duration rainfall (SDR) and long-duration rainfall (LDR) for the first period (2036–2065)

	Change in SDR (%)		Change in LDR (%)	
	Return periods		Return periods	
GCMs and Scenarios (2036–2065)	10-year	100-year	10-year	100-year
HadGEM2-ES RCP4.5	91.16	80.33	85.48	52.21
HadGEM2-ES RCP8.5	96.06	87.07	81.16	46.33
ICHEC-EC-EARTH RCP4.5	44.85	36.75	5.94	−16.94
ICHEC-EC-EARTH RCP8.5	35.48	26.92	12.69	−11.77
IPSL-IPSL-CM5A-MR RCP4.5	29.12	16.27	10.77	−13.58
IPSL-IPSL-CM5A-MR RCP8.5	42.97	33.55	14.88	−8.80
NorESM-1M RCP4.5	43.58	36.95	6.62	−16.29
NorESM-1M RCP8.5	32.30	19.53	1.79	−22.84

Table 8 | Average percentage changes of future IDF values (mm/h) compared with TSMS IDF values (mm/h) in terms of short-duration rainfall (SDR) and long-duration rainfall (LDR) for the second period (2066–2095)

	Change in SDR (%)		Change in LDR (%)	
	Return periods		Return periods	
GCMs and Scenarios (2066–2095)	10-year	100-year	10-year	100-year
HadGEM2-ES RCP4.5	116.76	82.66	95.71	40.14
HadGEM2-ES RCP8.5	113.60	85.81	97.99	44.16
ICHEC-EC-EARTH RCP4.5	17.31	5.11	−2.74	−28.29
ICHEC-EC-EARTH RCP8.5	30.96	22.31	24.72	−0.97
IPSL-IPSL-CM5A-MR RCP4.5	41.99	33.18	19.81	−5.02
IPSL-IPSL-CM5A-MR RCP8.5	41.38	30.69	21.39	−5.31
NorESM-1M RCP4.5	39.48	27.79	21.39	−5.31
NorESM-1M RCP8.5	44.73	29.98	17.26	−10.58

2066–2095. RCP4.5 rainfall intensities could decrease below and increase above RCP8.5. However, RCP8.5 scenarios generally have higher intensities than RCP4.5. Similar to Table 6, rainfall intensities for smaller periods will increase more than longer periods for short-duration rainfalls. When both the near and distant futures are compared, 10-year rainfall intensities in the distant future tend to increase more than the near future for all RCPs of HadGEM2-ES and ICHEC-EC-EARTH. For other GCMs, there is no constant tendency for the increases since they are changing depending on RCPs and GCMs.

For long durations, we can see that HadGEM2-ES models have the highest increases compared with other GCMs. The highest increase in the near future for 10-year and 100-year belongs to HadGEM2-ES RCP4.5 with 85.48 and 52.21%, respectively. For the distant future, HadGEM2-ES RCP8.5 scenarios show the highest change for 10-year and 100-year return periods with 97.99 and 44.16%, respectively. Contrary to short durations, all GCMs except HadGEM2-ES tend to see a reduction in rainfall intensities for the 100-year return period for both future periods. For the 10-year return period, only ICHEC-EC-EARTH under RCP4.5 is showing a decline for 10-year in the distant future. Therefore, we see higher increases for smaller return periods compared with the 100-year return period for longer durations. This finding also supports the findings of Table 6. NorESM1-M has the highest decrease in the near future, while ICHEC-EC-EARTH under RCP4.5 is decreasing more than others for the distant future. The range of changes in 10-year short-duration rainfall intensities are between 29.12 and 96.06%, and 30.96 and 116.76% for the near future and distant future, respectively. In the short duration of the 100-year return period, the range of changes in the near future is between 16.27 and 87.07%, and for the distant future, the range is between 5.11 and 85.81%.

Downloaded from http://iwaponline.com/jwcc/article-pdf/13/2/684/1013633/jwc0130684.pdf
by guest

Average percentage changes for two return periods (10-year and 100-year) and six durations (5 min, 15 min, 1 h, 3 h, 6 h and 24 h) are shown in Figure 9. It shows the percentages for selected durations and return periods for each GCM. For comparison, 5, 15 min and 1, 3-h rainfalls were selected to represent short-duration, 6 and 24-h rainfalls were selected for long-

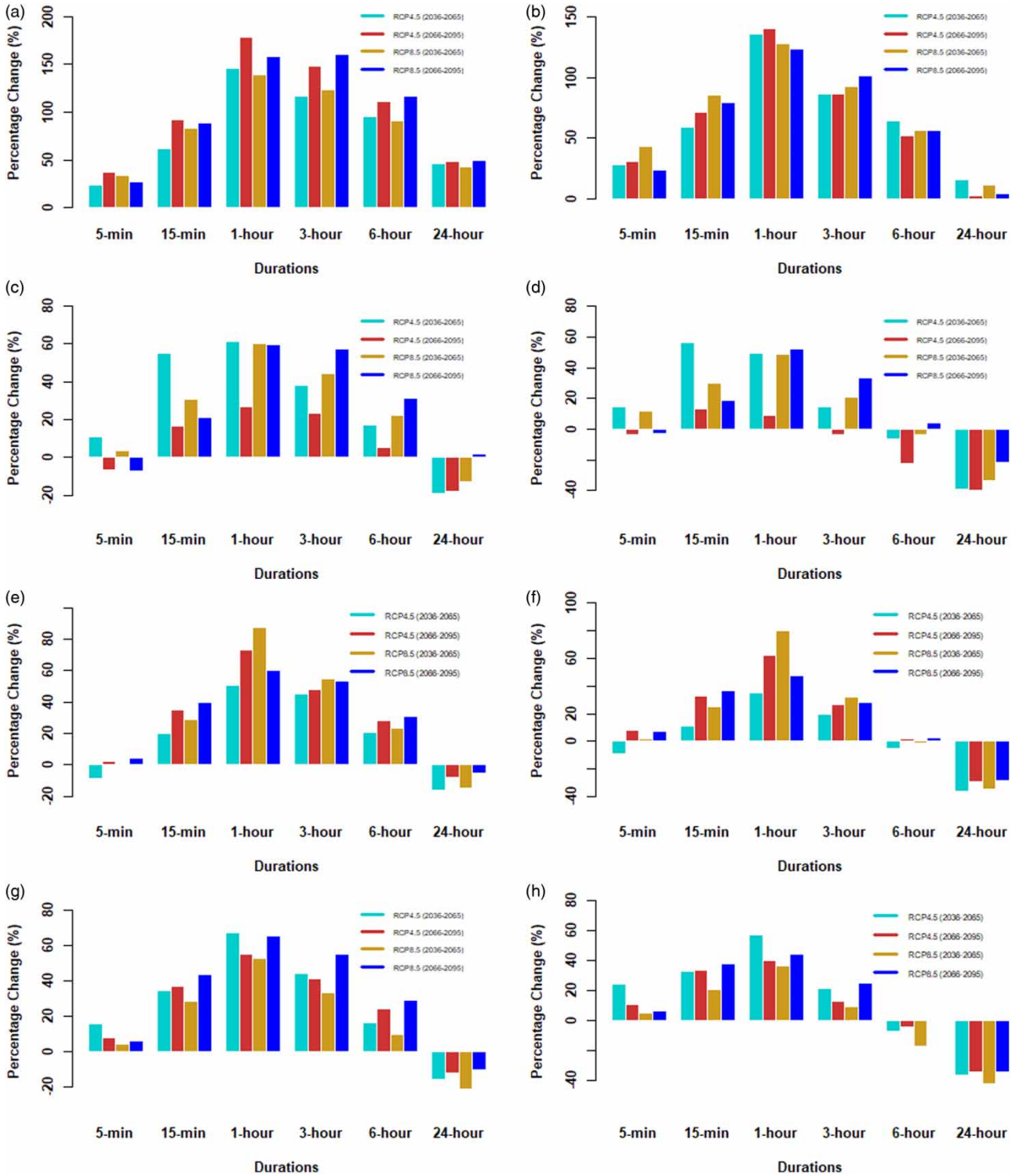


Figure 9 | Average percentage changes for different durations, periods and RCPs for (a) HadGEM2-ES 10-year return period, (b) HadGEM2-ES 100-year return period, (c) ICHEC-EC-EARTH 10-year return period, (d) ICHEC-EC-EARTH 100-year return period, (e) IPSL-IPSL-CM5A-MR 10-year return period, (f) IPSL-IPSL-CM5A-MR 100-year return period, (g) NorESM1-M 10-year return period and (h) NorESM1-M 100-year return period.

Downloaded from http://iwaponline.com/jwcc/article-pdf/13/2/684/1013633/jwc0130684.pdf
by guest

duration rainfalls. As mentioned in the findings of Tables 6–8, a great majority of short-duration rainfall intensities except several GCMs tend to increase in the future. It is also apparent that long-duration rainfall intensities, especially in 24-h, are encountering a great decline for all GCMs. However, 6-h values are increasing for most GCMs. As seen from Figure 9, HadGEM2-ES is the only one with a continuous increase. Another significant finding in Figure 9 is that 1-h values show increases more than other selected durations for all GCMs.

These analyses conclude that we will see highly intensified rainfalls for short-duration (less than 4 h) both in the near and distant futures, while the same cannot be said for long durations. Besides, increases in 10-year return periods are higher than the 100-year return period, which means that rainfall intensities that we are more likely to see will be greater than the rare rainfall intensities for both short and long durations, and for both future periods. The chance of rainfall intensities decreasing in the future is low. The most interesting aspect of the findings is we can see much higher short-duration rainfalls with a high possibility in both the near and distant futures.

Since there will be 16 IDF curve plots, we decided to reduce plot numbers to be shown by eliminating half of them. Rainfall intensity trends for TSMS IDF and future IDF curves are shown in Figure 10. The figure shows the various combinations of IDF curves generated with different RCPs and future periods (2036–2065) and (2066–2095) for all GCMs.

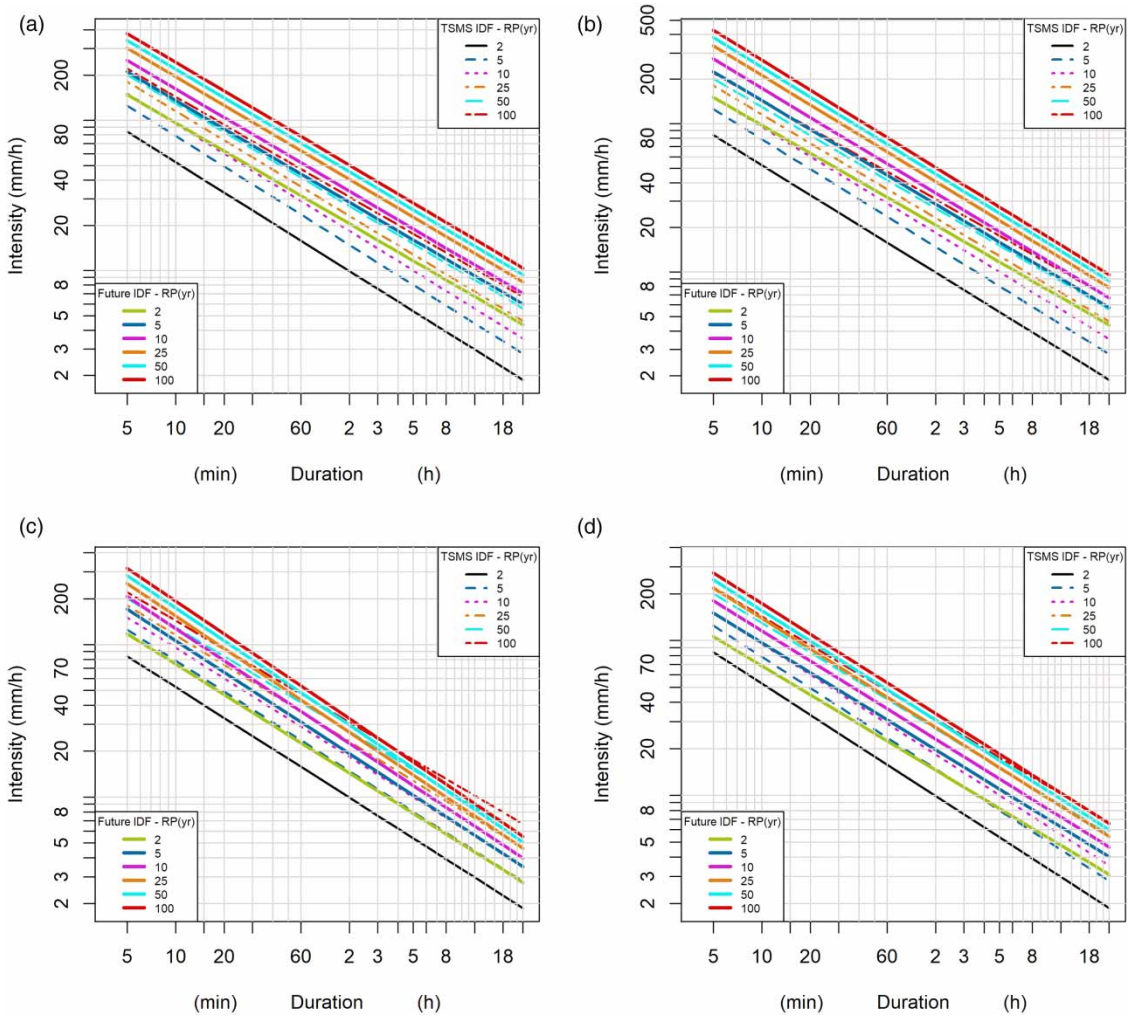


Figure 10 | IDF curve trends for selected future GCMs, periods, and RCPs compared to TSMS IDF curves: (a) TSMS vs HadGEM2-ES RCP4.5 (2036-2065), (b) TSMS vs HadGEM2-ES RCP8.5 (2036-2065), (c) TSMS vs ICHEC-EC-EARTH RCP8.5 (2036-2065), (d) TSMS vs ICHEC-EC-EARTH RCP8.5 (2066-2095), (e) TSMS vs IPSL-IPSL-CM5A-MR RCP4.5 (2066-2095), (f) TSMS vs IPSL-IPSL-CM5A-MR RCP8.5 (2066-2095), (g) TSMS vs NorESM1-M RCP4.5 (2036-2065) and (h) TSMS vs NorESM1-M RCP4.5 (2066-2095) (*Continued*).

Downloaded from http://iwaponline.com/jwcc/article-pdf/13/2/684/1013633/jwc0130684.pdf
by guest

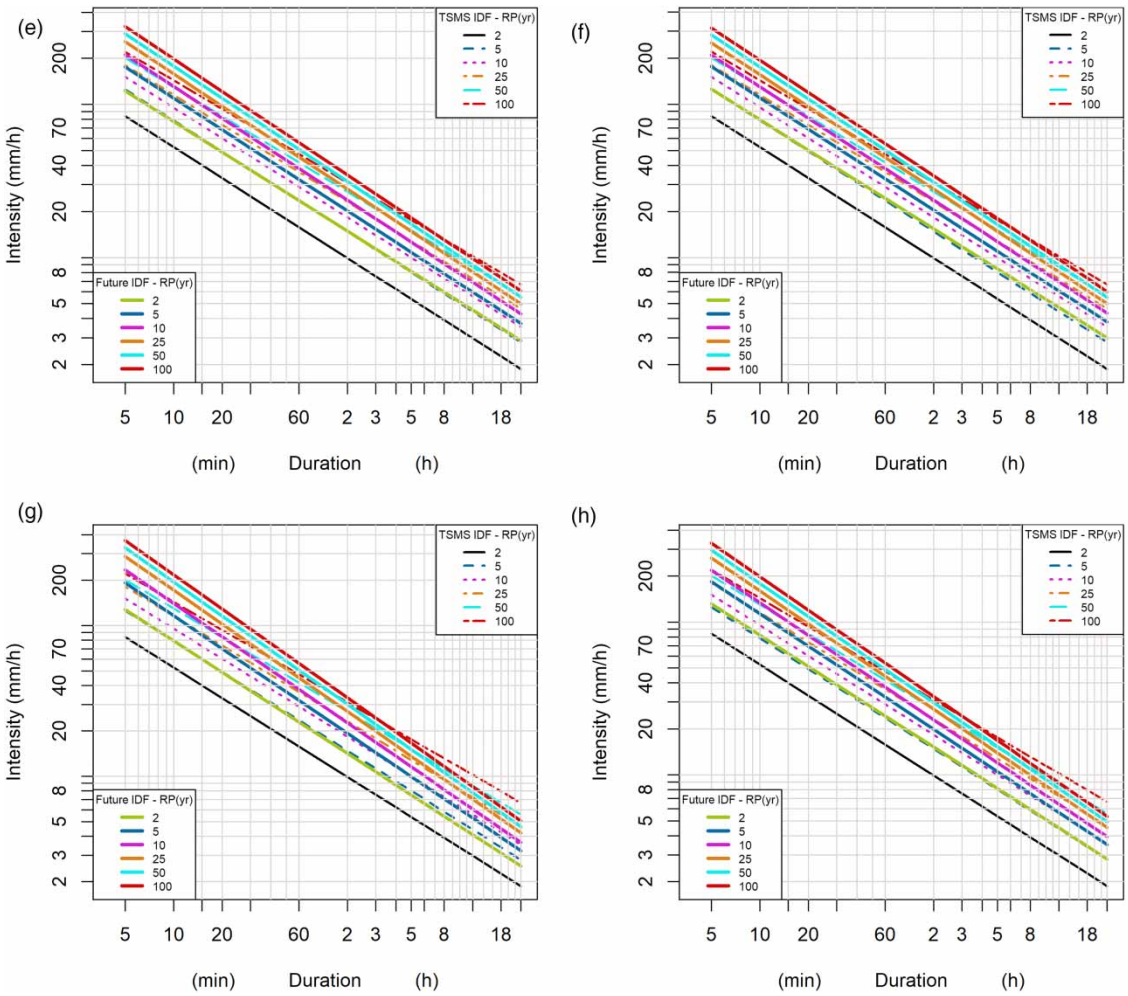


Figure 10 | (*Continued.*).

7. CONCLUSION

The aim of the present study was to generate reliable and updated rainfall IDF curves to be used as a serviceable tool in designing urban drainage systems against urban floods. Rainfall IDF curves play a crucial role in assessing flood risk and quantifying heavy rainfalls. IDF curves are also effective tools in designing and operating urban drainage systems. Since flash floods occur due to short-duration and high intensity rainfalls, the assessment of short-duration rainfalls was a major necessity. Hence, the first objective of the study was to generate IDF curves with both short-duration (less than 4 h) and long-duration (4 h and longer than 4 h) rainfalls. However, generating stationary IDF curves is not reliable in the assessment of floods since the climate of our world is changing continuously. Rainfalls are getting heavier due to climate change and floods are getting more hazardous for human life and cities. Besides, urbanization is also increasing impermeable surfaces and enabling floods to be more destructive. Therefore, IDF curves were generated especially for short-duration rainfalls to cope with all negative effects of climate change, urbanization, and insufficient drainage systems.

In the study, an ensemble of four GCMs, HadGEM2-ES, ICHEC-EC-EARTH, IPSL-IPSL-CM5A-MR and NorESM1-M, were provided for two different future periods 2036–2065 and 2066–2095. RCP4.5 and RCP8.5 scenarios were selected to obtain GCMs to represent future daily rainfall data. Since GCMs are not suitable to use directly due to biases, a bias-correction process was done. The distribution mapping method performed well (NSE ranges between 0.87 and 0.98) to adjust biases between measured and historical raw data.

In this study, disaggregation parameters were obtained from 14-year measured hourly rainfall, and parameter sets were determined for each month using some statistical measures. Afterwards, the determined parameters were applied for the

Downloaded from http://iwaponline.com/jwcc/article-pdf/13/2/684/1013633/jwc0130684.pdf
by guest

disaggregation of measured (applied to test the method) and future daily rainfalls. Hence, this process gives a chance for future data to capture historical patterns of selected region's rainfall instead of random rainfall characteristics. The results concluded that there is a close relationship between maximum values of TSMS measured rainfalls and maximum values of disaggregated rainfalls. Briefly, it is possible to disaggregate any daily rainfalls of a large region or city using only short records of hourly rainfall.

The results have shown that we will see much higher increases in short-duration rainfall intensities compared with longer durations for both the near and distant futures. Long-duration rainfalls tend to increase for 10-year return periods, while there are declines for the 100-year period for all GCMs except for HadGEM2-ES. These increases in short-duration rainfall intensities are valid for smaller and longer return periods. However, increases in smaller return periods are higher than longer return periods. This means that rainfall intensities that we are more likely to see will be greater than the rare rainfall intensities. Increases in short-duration rainfall intensity rise to 96.06% for 2036–2065 and 116.76% for 2066–2095, respectively. The main conclusion of the study is that short-duration rainfalls will be intensified in the near and distant future with a high possibility.

The importance of short-duration rainfalls on urban floods was explained in the previous sections. Long-duration rainfalls usually cause slower and less hazardous floods compared with short-duration floods. On the contrary, flash floods are increasing and getting more hazardous day after day. Hence, based on the results that the short-duration rainfalls will be more intensified, it is strongly recommended to use updated IDF curves in the assessment of flood risk, designing, and operating of urban drainage systems. In addition, flood management standards in cities must be rearranged considering IDF curves.

This study once again proved the need to use an updated IDF curve, which is generated under future climate conditions, for hydrology, hydraulic, and other water-related applications. The results also prove the necessity of selecting several GCMs for the analyses since every GCM shows major differences to others. Likewise, different disaggregation methods can simulate sub-hourly rainfall data in different ways. Therefore, future studies can be performed for more stations to enrich the awareness of climate change by evaluating more GCMs, disaggregation methods, and distribution functions.

DATA AVAILABILITY STATEMENT

Data cannot be made publicly available; readers should contact the corresponding author for details.

REFERENCES

BBC Weather 2020 *Weather – Istanbul*. Available from: https://www.bbc.com/weather/745044.

Berhanu, B., Seleshi, Y., Demisse, S. S. & Melesse, A. M. 2016 Bias correction and characterization of climate forecast system re-analysis daily precipitation in Ethiopia using fuzzy overlay. *Meteorological Applications* **23** (2), 230–243.

Cheng, L. & AghaKouchak, A. 2014 Nonstationary precipitation intensity-duration-frequency curves for infrastructure design in a changing climate. *Scientific Reports* **4** (1), 1–6.

Chow, V. T. 1951 A general formula for hydrologic frequency analysis. *Eos, Transactions American Geophysical Union* **32** (2), 231–237.

de Souza Costa, C. E. A., Blanco, C. J. C. & de Oliveira-Júnior, J. F. 2020 IDF curves for future climate scenarios in a locality of the Tapajós Basin, Amazon, Brazil. *Journal of Water and Climate Change* **11** (3), 760–770. https://doi.org/10.2166/wcc.2019.202.

Edenhofer, O., Pichs-Madruga, R., Sokona, Y., Minx, J. C., Farahani, E., Kadner, S. & Seyboth, K. 2015 Climate Change 2014 Mitigation of Climate Change Summary for Policymakers and Technical Summary, Working Group III Contribution to the Fifth Assessment Report of the Intergovernmental Panel on Climate Change (IPCC). In: *Annual Review of Environment and Resources*, Vol. 40, Issue 1. Available from: http://www.annualreviews.org/doi/10.1146/annurev-environ-021113-095626.

Hajani, E. 2020 Climate change and its influence on design rainfall at-site in New South Wales State, Australia. *Journal of Water and Climate Change* **11** (S1), 251–269.

Hanaish, I. S., Ibrahim, K. & Jemain, A. A. 2011 Daily rainfall disaggregation using HYETOS model for Peninsular Malaysia. *Matrix* **2**, 1.

Hosseinzadehtalaei, P., Tabari, H. & Willems, P. 2020 Climate change impact on short-duration extreme precipitation and intensity–duration–frequency curves over Europe. *Journal of Hydrology* **590**, 125249.

IPCC. 2014 *Climate Change 2014: Synthesis Report. Contribution of Working Groups I, II and III to the Fifth Assessment Report of the Intergovernmental Panel on Climate Change* (R. K. Pachauri & L.A. Meyer eds.). IPCC, Geneva, Switzerland.

Koutsoyiannis, D. & Onof, C. 2001 Rainfall disaggregation using adjusting procedures on a Poisson cluster model. *Journal of Hydrology* **246** (1–4), 109–122. https://doi.org/10.1016/S0022-1694(01)00363-8.

Mirhosseini, G., Srivastava, P. & Stefanova, L. 2013 The impact of climate change on rainfall Intensity–Duration–Frequency (IDF) curves in Alabama. *Regional Environmental Change* **13** (S1), 25–33. https://doi.org/10.1007/s10113-012-0375-5.

Nash, J. E. & Sutcliffe, J. V. 1970 River flow forecasting through conceptual models. Part I—a discussion of principles. *Journal of Hydrology* **10** (3), 282–290.

Downloaded from http://iwaponline.com/jwcc/article-pdf/13/2/684/1013633/jwc0130684.pdf
by guest

Nasim, W., Amin, A., Fahad, S., Awais, M., Khan, N., Mubeen, M., Wahid, A., Rehman, M. H., Ihsan, M. Z. & Ahmad, S. 2018 Future risk assessment by estimating historical heat wave trends with projected heat accumulation using SimCLIM climate model in Pakistan. *Atmospheric Research* **205**, 118–133.

Nwaogazie, I. L., Sam, M. G., Enciso, R. Z. & Gonsalves, E. 2019 Probability and non-probability rainfall intensity-duration-frequency modeling for Port-Harcourt metropolis, Nigeria. *International Journal of Hydrology* **3** (1). https://doi.org/10.15406/ijh.2019.03.00164.

Oyebande, L. 1982 Deriving rainfall intensity-duration-frequency relationships and estimates for regions with inadequate data. *Hydrological Sciences Journal* **27** (3), 353–367.

Rathjens, H., Bieger, K., Srinivasan, R. & Arnold, J. G. 2016 *CMhyd User Manual Documentation for Preparing Simulated Climate Change Data for Hydrologic Impact Studies*.

Rodriguez-Iturbe, I., Cox, D. R. & Isham, V. 1987 Some models for rainfall based on stochastic point processes. *Proceedings of the Royal Society of London A: Mathematical and Physical Sciences* **410** (1839), 269–288.

Rodriguez-Iturbe, I., Cox, D. R. & Isham, V. 1988 A point process model for rainfall: further developments. *Proceedings of the Royal Society of London A: Mathematical and Physical Sciences* **417** (1853), 283–298.

Sarhadi, A. & Soulis, E. D. 2017 Time-varying extreme rainfall intensity-duration-frequency curves in a changing climate. *Geophysical Research Letters* **44** (5), 2454–2463.

Singh, R., Arya, D. S., Taxak, A. K. & Vojinovic, Z. 2016 Potential impact of climate change on rainfall intensity-duration-frequency curves in Roorkee, India. *Water Resources Management* **30** (13), 4603–4616. https://doi.org/10.1007/s11269-016-1441-4.

Teutschbein, C. & Seibert, J. 2010 Regional climate models for hydrological impact studies at the catchment scale: a review of recent modeling strategies. *Geography Compass* **4** (7), 834–860. https://doi.org/10.1111/j.1749-8198.2010.00357.x.

Thom, H. C. S. 1958 A note on the gamma distribution. *Monthly Weather Review* **86** (4), 117–122.

Turkish State Meteorological Service 2020 *Resmi İstatistikler (İl ve İlçelerimize Ait İstatistiki Veriler)*. Available from: https://web.archive.org/web/20180422234324/https:/mgm.gov.tr/veridegerlendirme/il-ve-ilceler-istatistik.aspx?k=A&m=ISTANBUL.

Xin, X., Zhang, L., Zhang, J., Wu, T. & Fang, Y. 2013 Climate change projections over East Asia with BBC_CSM1.1 climate model under RCP scenarios. *Journal of the Meteorological Society of Japan* **91** (4), 413–429. https://doi.org/10.2151/jmsj.2013-401.

Zhu, J., Stone, M. C. & Forsee, W. 2012 Analysis of potential impacts of climate change on intensity–duration–frequency (IDF) relationships for six regions in the United States. *Journal of Water and Climate Change* **3** (3), 185–196. https://doi.org/10.2166/wcc.2012.045.

First received 15 June 2021; accepted in revised form 21 October 2021. Available online 29 October 2021

Downloaded from http://iwaponline.com/jwcc/article-pdf/13/2/684/1013633/jwc0130684.pdf
by guest